9-2001

Determining Matric Stress with the Modified Cam Clay Energy Relationship

Richard A. Rohlf
Kentucky Department for Surface Mining Reclamation and Enforcement

Larry G. Wells
University of Kentucky, larry.wells@uky.edu

Digital Object Identifier (DOI)
https://doi.org/10.13031/2013.6426

DETERMINING MATRIC STRESS WITH THE MODIFIED CAM CLAY ENERGY RELATIONSHIP

R. A. Rohlf, L. G. Wells

ABSTRACT. *The stress generated by matric suction, or matric stress, was determined at points along the stress path with an analytical and experimental procedure based on the modified Cam clay energy relationship. Matric stress was found to be approximately constant at large strain for constant water content triaxial compression tests. Matric stress was included in both shear and volume relationships in a critical–state soil model that employed the modified Cam clay yield function. Shear was modeled with a constant matric stress. Slope of the normal compression and recompression lines was adjusted for matric stress using a state function that expressed matric stress as a function of void ratio and degree of saturation. Predictions generated by the model for deviator stress and axial, lateral, and volumetric strain showed satisfactory agreement with data obtained from triaxial tests conducted on samples containing a range of void ratios and water contents.*

Keywords. *Unsaturated soil mechanics, Matric suction, Matric stress, Finite element model, Modified Cam clay, Triaxial testing.*

The analysis of unsaturated soils is complicated by the existence of negative pore water pressures, which can significantly affect mechanical behavior. Since the 1950s, a considerable amount of research has been devoted to describing the behavior of unsaturated soils. Past research has included: (1) the development of effective stress relationships for unsaturated soils, (2) the identification of independent stress state variables to describe the behavior of unsaturated soils, (3) the development of failure envelopes based on independent stress state variables, (4) the formulation of constitutive relationships for shear and volume behavior using independent stress state variables, and (5) the definition of matric stress, the stress generated by matric suction, as a component of the intergranular stress tensor with the determination of matric stress by indirect methods.

The objective of this article is to develop an analytical and experimental procedure for determining matric stress. Matric stress is defined through the intergranular stress tensor and determined with the modified Cam clay energy relationship. Matric stress is included in shear and volume relationships in a finite element model that employs a critical–state constitutive relationship, and the model is used to simulate the shear and strain response of unsaturated soil triaxial tests for a range of void ratios and water contents.

Article was submitted for review in February 2000; approved for publication by the Power & Machinery Division of ASAE in June 2001.

The investigation reported in this article (00–05–30) is part of a study by the Kentucky Agricultural Experiment Station and is published with the approval of the Director. Mention of any trade names is for informational purposes only and does not necessarily imply endorsement by the Kentucky Agricultural Experiment Station.

The authors are **Richard A. Rohlf**, Environmental Engineer Consultant, Kentucky Department for Surface Mining Reclamation and Enforcement, Frankfort, Kentucky; and **Larry G. Wells,** ***ASAE Member Engineer***, Professor, Department of Biosystems and Agricultural Engineering, University of Kentucky, Lexington, Kentucky. **Corresponding author**: Larry G. Wells, Department of Biosystems and Agricultural Engineering, Univ. of Kentucky, 128 Ag. Eng. Bldg., Lexington, KY 40546–0276; phone: 606–257–7381, ext. 219; fax: 606–257–5671; e–mail: lwells@bae.uky.edu.

PREVIOUS WORK

Summaries of past research related to the development of stress state variables and constitutive relationships for unsaturated soils can be found in Fredlund and Rahardjo (1993), Alonso et al. (1990), Toll (1990), and Lloret and Alonso (1980). Initial research focused on the development of an effective stress equation similar to that used for saturated soils. An important early relationship was that proposed by Bishop and co–workers (Bishop, 1959; Bishop et al., 1960; Bishop and Blight, 1963).

Primarily due to difficulties in predicting volume change behavior, the search for an effective stress relationship was gradually abandoned in favor of independent stress state variables (Jennings and Burland, 1962; Bishop and Blight, 1963; Burland, 1965; Blight, 1967; Matyas and Radhakrishna, 1968). Fredlund and Morgenstern (1977) proposed the use of net stress, $(\sigma_{ij} - u_a\delta_{ij})$, and matric suction, $(u_a - u_w)\delta_{ij}$, where σ_{ij} is the total stress tensor, u_w is pore–water pressure, u_a is pore–air pressure, and δ_{ij} is the Kronecker delta. Fredlund et al. (1978) proposed a Mohr–Coloumb failure envelope that incorporated these two stress state variables.

Lloret and Alonso (1980) coupled the one–dimensional air and water continuity equations with state surfaces for void ratio and degree of saturation to develop a model for volume change behavior including swelling and collapse. The state surfaces for void ratio and degree of saturation were functions of the independent stress variables $(\sigma - u_a)$ and $(u_a - u_w)$.

Karube (1988) described matric suction as an internal stress component that can be included in constitutive relationships without explicit addition as an independent stress state variable. For soils in which apparent cohesion was

  ISSN 0001–2351

assumed to be a function of matric suction only, Karube proposed that the ultimate strength envelope be defined by:

$$q_f = M[p_a + f(\mu)] \quad (1)$$

where

q_f = deviator stress at failure, $(\sigma_1 - \sigma_3)$
p_a = mean net stress, $[(\sigma_1 + 2\sigma_3) / 3] - u_a$
$f(\mu)$ = function that converts matric suction, μ, into mean stress
M = slope of the failure line
σ_1 and σ_3 = major and minor principal stresses, respectively.

Karube also investigated volume behavior for isotropic compression by replacing $\overline{p_a}$ with the term $\overline{p_a} + f(\mu)$ in the coefficient of volume change equation:

$$m_v = \frac{0.434 C_c}{1+e} \frac{1}{\overline{p_a}} \quad (2)$$

where

m_v = coefficient of volume compressibility
C_c = compression index
$\overline{p_a}$ = average mean net stress for an incremental increase in p_a
e = void ratio.

Alonso et al. (1990) developed a constitutive model that addresses some of the basic observed behaviors of unsaturated soil including: (1) compression stiffness variation with changes in matric suction, (2) variation in amount of collapse as a function of stiffness and hence matric suction, and (3) irreversible response under stress and suction reversals. The model was formulated using the independent stress state variables $(\sigma - u_a)$ and $(u_a - u_w)$ and incorporated separate volume change relationships for mean stress and matric suction. The yield surface was also formulated as a function of both mean stress and matric suction. The model requires a total of ten material constants for full implementation and reduces to the modified Cam clay at saturation.

Toll (1990) proposed a critical–state framework for unsaturated soils that was formulated in terms of the independent stress state variables $(\sigma - u_a)$ and $(u_a - u_w)$ and the volumetric variable of specific volume.

Wheeler and Sivakumar (1995) proposed an elastoplastic critical–state framework for unsaturated soil based on data from controlled suction triaxial tests. The framework was formulated in terms of the state variables of mean net stress, deviator stress, matric suction, and specific volume. Within this four–dimensional space, a normal compression line, critical–state line, and state boundary surface were defined. An associated flow rule and yield surface similar to the modified Cam clay model were assumed.

Adams and Wulfsohn (1997, 1998) evaluated the applicability of critical–state theory for unsaturated soil mechanics problems encountered in agriculture. The evaluation was conducted using the state variables of mean net stress, deviator stress, matric suction, and specific volume. Constant water content and constant matric suction triaxial tests were conducted on an unsaturated sandy clay loam. A unique critical–state line was established for constant matric suction tests, while constant water content tests did not attain critical state for confining pressures greater than the matric suction of 50 kPa. For constant water content tests, matric suction was found to be approximately constant during shearing for lower confining stresses (<70 kPa). Slope of the critical–state line, M, did not vary with matric suction for samples prepared with the same structure, but M did vary for samples prepared with different structures.

Rohlf et al. (1997) used the intergranular stress tensor developed by Matyas and Radhakrishna (1968) to define matric stress as the stress generated by matric suction. By applying equilibrium conditions along a curved surface normal to solid contact points in an unsaturated soil matrix, Matyas and Radhakrishna (1968) showed that the intergranular stress could be expressed as:

$$\overline{\sigma_{ij}} = [p_a + A_w \mu + \int T dx]\delta_{ij} + S_{ij} \quad (3)$$

where

$\overline{\sigma_{ij}}$ = intergranular stress or equivalent stress transmitted by solid contacts
A_w = measure of pore space saturation
T = surface tension
x = perimeter of the air–water meniscus
S_{ij} = deviatoric stress.

Because $\int T dx$ is a function of water content and thus μ, equation 3 can be written:

$$\overline{\sigma_{ij}} = [p_a + f(\mu)]\delta_{ij} + S_{ij} \quad (4)$$

where

$$f(\mu) = A_w \mu + \int T dx \quad (5)$$

can be considered as a matric stress term.

Rohlf et al. (1997) employed Karube's (1988) basic formulation and treated matric stress as an applied confining stress. Matric stress was determined through an ultimate strength relationship. Plotting the deviator stress versus mean net stress, p_a, yields a failure line with slope M_a and cohesion intercept q_c:

$$q_f = M_a p_a + q_c \quad (6)$$

Plotting the deviator stress versus mean net stress plus matric stress, $p_a + f(\mu)$, yields a failure line with slope M and cohesion intercept of zero:

$$q_f = M\,[p_a + f(\mu)] \quad (7)$$

Equations 6 and 7 can be equated and the resulting relationship solved for matric stress at failure:

$$f(\mu) = \frac{[p_a(M_a - M) + q_c]}{M} \quad (8)$$

Additional details on the development of the ultimate strength matric stress formulation can be found in Rohlf et al. (1997).

Rohlf et al. (1997) included matric stress in both shear and volume relationships in a critical–state soil model that employed the modified Cam clay yield function. Shear was modeled using a constant matric stress, which was determined at critical state. The slope of the normal compression and recompression lines were adjusted for matric stress using a state function that expressed matric stress as a function of void ratio and degree of saturation. Model–predicted deviator stress and axial, lateral, and volumetric strain showed satisfactory agreement with data from triaxial tests.

Development of a Matric Stress Relationship

The developments presented in this article assume that the state of a soil element can be described by the stress tensor, $[\sigma_{ij} - u_a\delta_{ij} + f(\mu)\delta_{ij}]$, void ratio ($e$), water content ($w$), and soil fabric. Matric stress is treated as an applied confining stress.

Although matric suction can be measured directly, adequate methods for the direct measurement of matric stress are not yet available, requiring that matric stress be determined by indirect methods. The following section describes a methodology for determining matric stress from an energy relationship.

Energy Matric Stress Formulation

An energy matric stress relationship is developed under the following assumptions: (1) soil has no true cohesion, (2) apparent cohesion is due to matric stress only, (3) slope of the failure line, M, is independent of degree of saturation, and (4) soil behavior is described by the modified Cam clay model. The first and second assumptions eliminate from consideration cemented soils and soils that exhibit cohesion due to electrochemical forces between soil particles. The third assumption removes the requirement for separate friction parameters for mean net stress and matric stress or matric suction. The fourth assumption is needed because it is necessary to first adopt an energy relationship and then check the validity of the adopted model.

By following Karube's suggestion and replacing p_a with $p_a + f(\mu)$, the modified Cam clay work equation can be written (Roscoe and Burland, 1968):

$$\eta^2 + 2D\eta - M^2 = 0 \tag{9}$$

where

η = $q / [p_a + f(\mu)]$

D = plastic dilatancy, $d\varepsilon_v^p / d\varepsilon_s^p$

$d\varepsilon_v^p$ = incremental plastic volumetric strain

$d\varepsilon_s^p$ = incremental plastic shear strain.

Solving for η gives:

$$\eta = \frac{-2D + (4D^2 + 4M^2)^{1/2}}{2} \tag{10}$$

With η determined, matric stress can be calculated from:

$$f(\mu) = \frac{q - \eta p_a}{\eta} \tag{11}$$

Equations 10 and 11 allow matric stress to be calculated at any point along the stress path where q, p_a, D, and M are known.

Volume Behavior Matric Stress Formulation

Volume change matric stress relationships for unsaturated constant water content hydrostatic compression test conditions were presented by Rohlf et al.(1997) and are summarized below. Volume behavior considering mean net stress alone can be described by:

$$e = e_o - \lambda_a Ln(p_a / p_{ao}) \tag{12}$$

where λ_a is the slope of the normal compression line for mean net stress, and e_o is the void ratio at p_{ao}.

Volume behavior considering mean net stress and matric stress can be described by replacing p_a with $p_a + f(\mu)$ in the logarithmic compression relationship:

$$e = e_o - \lambda Ln\left[\frac{p_a + f(\mu)}{p_{ao} + f(\mu)_o}\right] \tag{13}$$

where λ is the slope of the normal compression line, and e_o is the void ratio at $p_{ao} + f(\mu)_o$ (Karube, 1988).

Eliminating void ratio differences in equations 12 and 13 and solving for λ gives:

$$\lambda = \lambda_a \frac{Ln\left[\frac{p_a}{p_{ao}}\right]}{Ln\left[\frac{p_a + f(\mu)}{p_{ao} + f(\mu)_o}\right]} \tag{14}$$

thus correcting λ_a for the effects of matric stress. Relationships analogous to equations 12 through 14 were also assumed to hold in the recompression stress range.

Soil Testing and Determination of Parameters

Project Background

Development of a matric stress relationship was part of a larger project to measure and analytically model the mechanical behavior of unsaturated rill and gully sized channel banks (100 mm to 300 mm in depth) subjected to water level changes. The project consisted of laboratory experiments, development of relationships to determine the stress generated by negative pore–water pressure, and analytic modeling of channel bank failure (Rohlf, 1993).

Laboratory experiments to investigate the behavior of channel banks were conducted using a Plexiglas flume (900 mm long × 250 mm high × 152 mm wide) that was divided into a soil compartment and a water compartment by a removable Plexiglas retaining wall. Laboratory experiments consisted of compacting soil in the flume, removing the retaining wall, and running water in the flume along the exposed channel bank face. Video and 35 mm photographs recorded the advancing wetting front and slope failure mechanism, and soil samples were taken to determine the vertical and longitudinal water content distribution.

Sample Preparation and Testing Methodology

Samples for triaxial and hydrostatic testing were prepared by: (1) gradually and uniformly mixing a predetermined amount of water and air–dried soil to achieve the desired water content, (2) placing soil in sample molds in approximately 50 mm layers, and (3) compacting the sample to the desired density using a cyclic soil compactor. After compaction, samples were sealed in a plastic container and stored in a high–humidity chamber. Samples were allowed to equilibrate for a minimum of 12 hours prior to testing.

Maury silt loam (CL; LL = 34, PI = 10) was used for all laboratory experiments and soil strength tests. Maury soil formed primarily from weathered phosphatic limestone, but also partly from a mantle of silt (Romkens et al. 1985). The soil was sieved through a #20 screen to remove all particle sizes greater than 0.84 mm. The particle size distribution

contained 27% clay (<0.002 mm), 65% silt (0.002 mm – 0.05 mm), and 8% sand (>0.05 mm).

Soil samples were formed in split cylindrical Plexiglas molds 50.8 mm in diameter by 250 mm in length. The 250 mm molds contained two sections 101.6 mm long and one section 46.8 mm long. Thus, each mold produced two 50.8 mm × 101.6 mm samples for triaxial testing. Five Plexiglas molds were prepared simultaneously to form sample sets containing ten samples. Sample sets were designated as S1 – S6 for sample sets 1 through 6, and FT1 – FT4 for samples prepared in conjunction with channel bank flume tests 1 through 4. Sample sets S1 through S3 were used to develop the triaxial testing methodology, and the remaining sample sets (S4 – S6 and FT1 – FT4) were separated by mold section (lower, upper) and used for triaxial shear tests, hydrostatic consolidation tests, permeability tests, and to develop soil–water characteristic curves. In addition, some samples were used to determine the uniformity of the sample preparation procedure and others were lost due to breakage. Individual samples were designated as T*xxx* or H*xxx* for triaxial shear or hydrostatic tests, respectively, where *xxx* designates the sample number.

Soil samples for triaxial and hydrostatic testing were compacted with a specially designed cyclic compactor. Cyclic compaction was selected because it was necessary to produce samples with a minimum amount of overconsolidation to duplicate normally consolidated soil conditions under which most rill and gully sized channel banks are formed, and to reduce the layering effect that can occur with impact or static load compaction techniques. Cyclic compaction relies on the principle that soils under drained conditions incur cumulative volumetric contraction when subjected to cyclic loading (Wood, 1990).

The average void ratio and water content for sample sets and mold sections (lower, upper) used in triaxial tests varied from 0.852 to 1.727, and from 23.4% to 28.4%, respectively. The average standard deviation for void ratio and water content within sample sets and mold sections for all samples were 0.041% and 0.4%, respectively. Thus, the sample preparation and compaction technique produced samples with reasonably uniform phase characteristics. Additional information on the sample preparation and testing procedures can be found in Rohlf et al. (1997).

Determination of Parameters for Matric Stress

As described in a previous section, application of equations 10 and 11 to calculate matric stress at points along the stress path requires that the parameters q, p_a, D, and M be determined. The deviator stress, q, and mean net stress, p_a, are determined directly from triaxial tests. Procedures for calculating the dilation, D, and slope of the critical–state line, M, are described below.

Representative curves of volumetric strain versus shear strain for four confined triaxial tests are presented in figure 1, where contraction is taken as positive. Because volumetric strains were large, they were computed by expanding the definition of volumetric strain for an axisymmetric stress state, $[1 - (1 - \varepsilon_1)(1 - \varepsilon_3)(1 - \varepsilon_3)]$, to give:

$$\varepsilon_v = \varepsilon_1 + 2\varepsilon_3 - 2\varepsilon_1\varepsilon_3 - \varepsilon_3^2 + \varepsilon_1\varepsilon_3^2 \qquad (15)$$

where ε_v is volumetric strain, ε_1 is axial strain, and ε_3 is lateral strain (Whitlow, 1990). Shear strains were computed with the modified Cam clay shear strain definition:

$$\varepsilon_s = \frac{2}{3}(\varepsilon_1 - \varepsilon_3) \qquad (16)$$

where ε_s is shear strain (Schofield and Wroth, 1968). Equations of the form:

$$\varepsilon_v = a_1\varepsilon_s^{b_1} \qquad (17)$$

and

$$\varepsilon_v = a_2 + b_2\ln(\varepsilon_s) + c_2\ln(\varepsilon_s)^2 + d_2\ln(\varepsilon_s)^3 \qquad (18a)$$

or

$$\varepsilon_v = a_3 + b_3\varepsilon_s + c_3\varepsilon_s^2 \qquad (18b)$$

where a_i, b_i, c_i, and d_i (i = 1,2,3) are regression coefficients, were fitted to the ε_v versus ε_s data sets and differentiated to determine sample dilation, D. Primarily due to the intercept, equation 18a or 18b did not always provide reasonable estimates of dilation at the lower points in the $\varepsilon_v - \varepsilon_s$ data sets. In these cases equation 17, which forces an intercept of zero, was fitted to the lower portion of the curve and used to determine dilation at the lower points. The semi–logarithmic relationship, equation 18a, generally gave better results than the polynomial, equation 18b. The second–degree form of equation 18a was sufficient in most cases. The average coefficient of determination, R^2, for equation 17 was 0.983, with a minimum R^2 of 0.929. The average coefficient of determination for equations 18a and 18b was 0.982, with a minimum R^2 of 0.941. No correction was made for elastic strain, and thus $d\varepsilon_v^p / d\varepsilon_s^p$ was assumed equal to $d\varepsilon_v / d\varepsilon_s$. Selected curves for equations 18a or 18b are presented in figure 1.

Slope of the critical–state line, M, was determined using a technique described in Rohlf et al. (1997) and summarized below. Failure lines in q–p_a space were developed using two points generated by an unsaturated, unconfined constant water content triaxial test, and an unsaturated, consolidated constant water content triaxial test at a confining pressure of

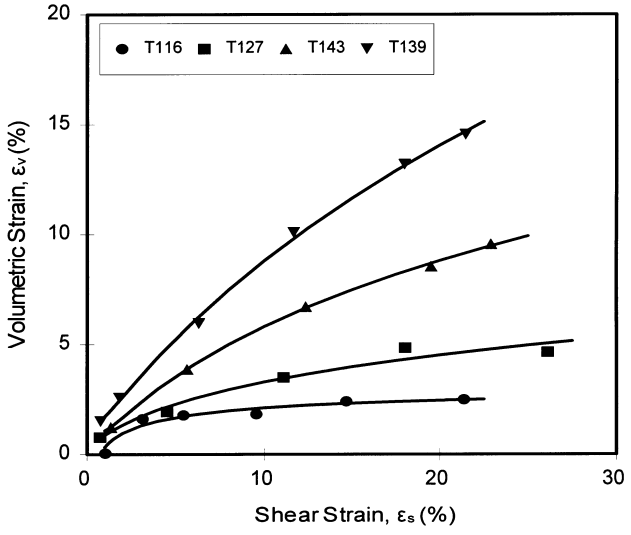

Figure 1. Curves of volumetric strain versus shear strain for determining dilation.

approximately 3.4 kPa or 6.9 kPa. All unconfined triaxial tests reached failure at axial strains ranging from 1.9% to 11.1%. Visual failure characteristics of unconfined samples ranged from bulging and cracking at the sample surface to massive collapse. Volumetric strain generally increased during shear (contraction positive). However, due to nonuniformity of volume change behavior for the unconfined samples, curves of volumetric strain exhibited large variations from any trend. Because the unconfined samples failed, it was assumed that they reached critical state, and the maximum deviator stress was taken as q_f.

Confined triaxial samples continued to deform uniformly during shear with no visible evidence of failure. Axial strains ranged from 21.0% to 29.7% at the termination of testing, with the majority of the tests exceeding 25% axial strain. All of the samples exhibited positive volumetric strain. Because confined samples were still consolidating at the termination of testing, the maximum deviator stress, q, was corrected for dilatancy using an energy correction procedure for unsaturated soils that employed the modified Cam clay energy relationship (Rohlf et al., 1997):

$$q_f = \frac{\frac{2Dq}{M} + \left[\frac{4D^2q^2}{M^2} + 4q^2\right]^{1/2}}{2} \tag{19}$$

The slope of the failure line considering mean net stress, p_a, only was calculated as:

$$M_a = \frac{q_2^f - q_1^f}{p_2 - p_1} \tag{20}$$

where

q_1^f and q_2^f and p_1 and p_2 are deviator stresses at failure and corresponding mean net stresses for the unconfined and confined triaxial tests, respectively. Slope of the critical–state line, M, was determined by projecting failure line slopes determined in q–p_a space to saturation using the relationship:

$$M_a = \exp[a_4 + b_4(1 - S_s)^2] \tag{21}$$

where S_s is degree of saturation at sample formation, and a_4 and b_4 are regression coefficients (Rohlf et al., 1997). At saturation:

$$M = \exp(a_4) \tag{22}$$

Additional details on the development of this procedure can be found in Rohlf et al. (1997)

Dilation, D, and slope of the failure line, M, as determined by the above procedures were used with equations 10 and 11 to calculate matric stress, f(μ), at each q, p_a point in the stress path. Selected graphs of matric stress versus shear strain are presented in figure 2. These relationships show that f(μ) varied considerably during the initial stages of shearing (ε_s < 10%) but then approached a relatively constant value.

Initial attempts to model triaxial tests using functions that approximated the f(μ) relationships displayed in figure 2 did not produce agreement between predicted and measured curves of deviator stress and axial strain. One of the assumptions underlying the procedure for determining matric stress, f(μ), is that soil behavior is described by the modified Cam clay model. Hydrostatic soil tests indicate that the soil compaction procedure produced some overconsolidation (Rohlf et al., 1997). Since soils behave elastically in the overconsolidated region, calculated values of f(μ) may not be correct, and thus use of the f(μ) relationships displayed in figure 2 to model triaxial tests would not produce agreement between predicted and measured results.

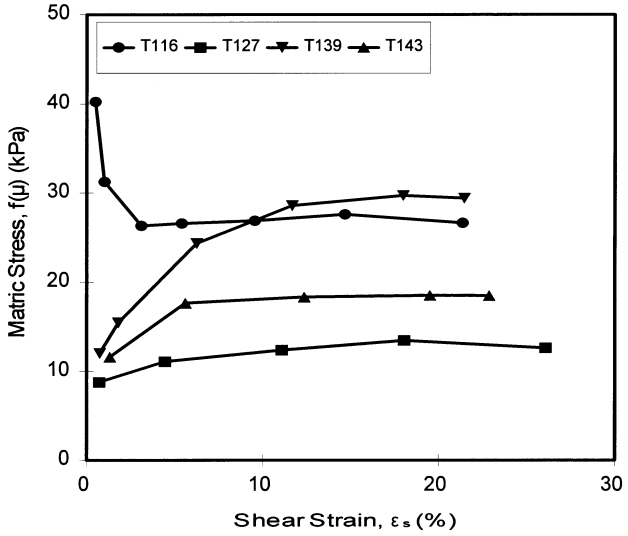

Figure 2. Matric stress versus shear strain along the stress path.

Because f(μ) approached an approximately constant value near the end of shearing, a simplifying assumption was made that f(μ) is constant throughout shearing, with f(μ) determined from an average of values near the end of the f(μ) – ε_s curves. Although it would be possible to calculate an average f(μ) using values from figure 2, where the f(μ) – ε_s curve is approximately level, there is no way of knowing if the selected points satisfy the modified Cam clay model.

To provide guidance in selecting f(μ) values for calculating an average, a procedure that compares measured soil behavior to ideal plastic behavior with constant f(μ) is developed. Curves of Atan($\bar{D}$) versus $\bar{\eta}$ are constructed by solving equation 9 for D:

$$\bar{D} = \frac{M^2 - \bar{\eta}^2}{2\bar{\eta}} \tag{23}$$

with

$$\bar{\eta} = \frac{q}{p_a + \overline{f(\mu)}} \tag{24}$$

where

$\bar{D}$, $\bar{\eta}$, and $\overline{f(\mu)}$ indicate average values, with $\overline{f(\mu)}$ determined from points near the end of the f(μ) – ε_s curves. Selected curves of Atan($\bar{D}$) versus $\bar{\eta}$ are plotted in figure 3 and labeled "plastic" to indicate that they represent ideal modified Cam clay plastic behavior for f(μ) constant throughout shearing. Note that the Atan($\bar{D}$) versus $\bar{\eta}$ relationships essentially plot as a single curve in figure 3. Second, curves of Atan($\bar{D}$) versus $\bar{\eta}$ were developed using $D = d\varepsilon_v / d\varepsilon_s$ determined from equations 17 and 18. These curves are included in figure 3 and labeled "calculated". Note

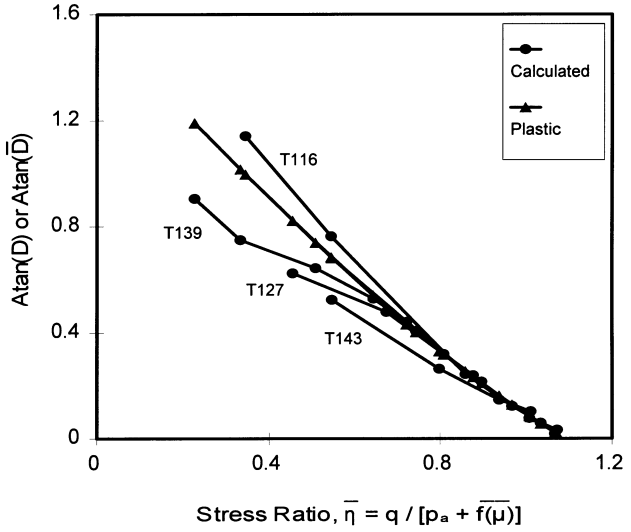

Figure 3. *A*tan(*D*) or *A*tan($\overline{D}$) versus $\overline{\eta}$ for selection of points to use in calculating $\overline{f(\mu)}$.

that since $D = d\varepsilon_v / d\varepsilon_s$ is used in determining $f(\mu)$, $\overline{D} = D$ when $\overline{f(\mu)}$ is determined from only one point.

Beginning at the highest shear strain, points were added successively in descending ε_s order, provided the "plastic" and "calculated" curves were approximately coincident over the ε_s range used in calculating $\overline{f(\mu)}$. Coincidence of the curves indicated agreement with the modified Cam clay energy relationship for $\overline{f(\mu)}$ determined from selected points near the end of the $f(\mu) - \varepsilon_s$ curves. The results of successively adding points to determine $\overline{f(\mu)}$ are displayed in figure 3. Average matric stress values determined with the above procedure, the number of points used in calculating $\overline{f(\mu)}$, and soil sample information are included in table 1 for confined triaxial tests.

Divergence of the curves in figure 3 could have resulted from a number of factors including: (1) elastic behavior at small and medium strains due to overconsolidation induced by the cyclic soil compaction procedure, (2) inaccurate measurement of small volumetric strain, (3) inaccuracy in the curve–fitting procedure and differentiation to determine dilation (*D*), and (4) soil behavior not satisfying the modified Cam clay energy relationship or an incorrect assumption that $f(\mu)$ is constant throughout shearing.

Determination of Parameters for Volume Behavior

As previously discussed, volume behavior resulting from the application of mean net stress and matric stress, $p_a + f(\mu)$, can be described by equations 12 through 14. Calculation of λ with equation 14 requires two values of mean net stress and matric stress at corresponding values of void ratio and degree of saturation. Because $f(\mu)$ as determined by equation 11 is in terms of q, p_a, D, and M, it is not convenient to use in adjusting the normal compression line. Consequently, a more general relationship or state function is needed for matric stress.

Results from the energy analysis were used to develop a state function for matric stress in terms of void ratio and degree of saturation. A regression analysis using $f(\mu)$ as determined with equation 11 and the above procedure, and accompanying values of void ratio and degree of saturation, produced:

$$f(\mu) = e^{-5.33} \exp[2.08 + 10.05(1 - S)^2] \qquad (25)$$

with $R^2 = 0.73$. Graphs of (a) equation 25, and (b) calculated $f(\mu)$ versus predicted $f(\mu)$ (eqs. 11 and 25) are provided in figure 4. Separate symbols used for the upper and lower mold sections in figure 4 indicate that there was no discernable trend in matric stress related to the two mold sections. With λ_a and w provided, equations 12, 14, and 25 can be used to calculate an average λ for a selected p_a pressure interval.

Simulation of Triaxial Tests

Selected triaxial tests were simulated with a two–dimensional saturated–unsaturated groundwater flow and elasto-plastic stress–strain finite element model. The model includes groundwater and soil constitutive relationships and is formulated in terms of fluid head and net stress plus matric stress. The soil constitutive relationship utilizes the modified Cam clay yield function. Matric stress is included in both shear and volume relationships. Body and phase interaction forces incorporated in the model include soil structure weight, fluid weight, and fluid drag.

Table 1. Average matric stress and sample parameters for triaxial tests.

Set	Test	e_s[a]	w	S_s[b]	Number of points[c]	$\overline{f(\mu)}$ (kPa)
S4–L[d]	T116	0.862	0.263	0.818	5	26.8
S5–L	T122	1.452	0.271	0.500	2	12.6
S6–L	T125	1.481	0.271	0.490	2	16.0
FT1–L	T127	1.021	0.284	0.745	3	12.8
FT1–U	T128	1.046	0.279	0.715	3	22.8
FT2–L	T132	1.137	0.285	0.672	2	14.9
FT2–U	T133	1.033	0.280	0.726	3	17.0
FT3–U[e]	T139	1.696	0.237	0.375	3	29.2
FT4–L	T143	1.406	0.250	0.477	4	18.3
FT4–U	T144	1.479	0.252	0.457	2	23.2

[a] Sample void ratio.
[b] Degree of saturation.
[c] Number of points used in calculating $\overline{f(\mu)}$.
[d] L designates the lower mold section and U designates the upper mold section.
[e] Due to breakage of samples during preparation for triaxial testing, there were no results for FT3–L.

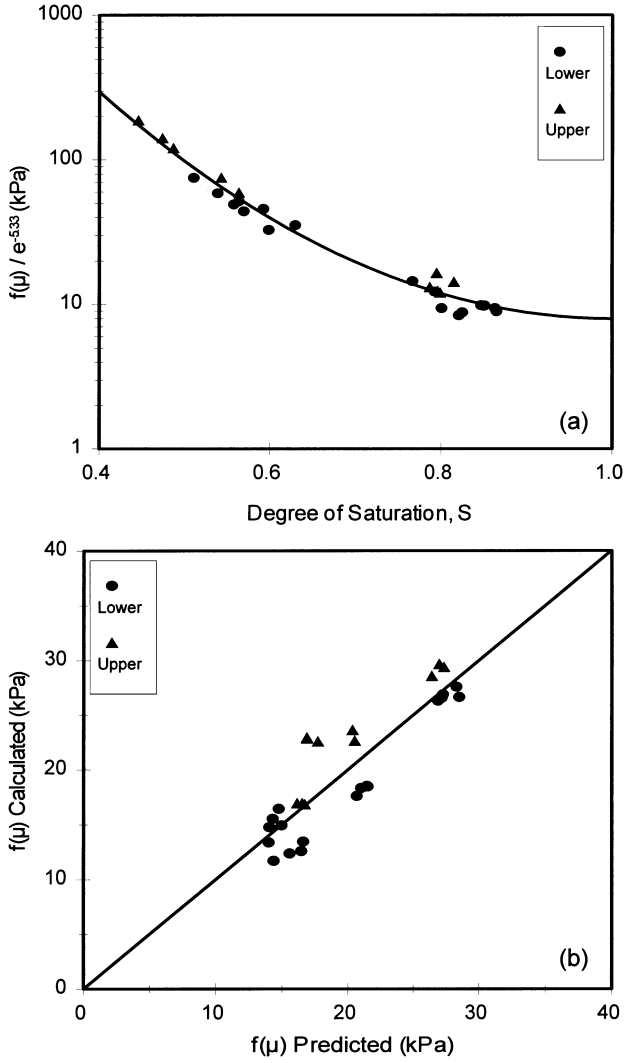

Figure 4. State function for matric stress (a) f(μ)/f(e) versus degree of saturation, and (b) calculated f(μ) versus predicted f(μ).

A Galerkin and finite difference solution is used for the groundwater equation, and a virtual displacement solution is used for the soil equation. The solution is uncoupled and loops over both the groundwater and soil equations until convergence is achieved. Additional information on the development of the model can be found in Rohlf et al. (1994) and Rohlf et al. (2000).

Four constant water content triaxial compression tests with varying initial void ratios and water contents were simulated with the finite element model. Average matric stress values contained in table 1 were used. Slope of the critical–state line, *M*, was determined as previously described. The parameters λ and κ (slope of the compression and unloading–reloading lines, respectively) were deter–mined from five hydrostatic compression tests conducted on unsaturated samples. Soil characteristics and values of λ_a and κ_a for these tests are reported in table 2.

Values of λ_a from these tests were corrected for matric stress using equation 14 for a mean net stress interval of 7 kPa to 30 kPa, the approximate pressure interval developed during triaxial testing. Similar corrections were made for κ_a over the mean net stress interval of 1 kPa to 30 kPa. The

Table 2. Lambda, kappa, and sample parameters for hydrostatic compression tests.

Set	Test	e_s	S_s	λ_a	κ_a
S4–L	H117	0.831	0.851	0.017	0.002
S6–L	H126	1.456	0.499	0.197	0.014
FT1–U	H131	1.043	0.704	0.047	0.008
FT2–U	H136	1.211	0.604	0.087	0.010
FT3–U	H140	1.777	0.353	0.284	0.016

adjusted λ and κ values are plotted versus sample void ratio in figure 5. Equations fitted to the λ and κ values in figure 5 include:

$$\lambda = \exp(-4.88 + 3.59e_s^2 - 1.22e_s^3) \quad (26)$$

and

$$\kappa = \exp(-7.97 + 5.43e_s - 1.35e_s^2) \quad (27)$$

where e_s is the sample void ratio. The coefficient of determination, R^2, for equations 26 and 27 was 0.99 and 0.98, respectively. Equations 26 and 27 were used to calculate λ and κ for each of the triaxial simulations.

Because preconsolidation pressures were not available for each sample set, an average mean net preconsolidation stress was calculated from the hydrostatic compression tests (p_{ao} = 11 kPa; Rohlf et al., 1997). Poisson's ratio was taken from Das (1983) and Young's modulus was calculated with:

$$E = \frac{3[p_a + f(\mu)](1+e)(1-2v)}{\kappa} \quad (28)$$

using average values of p_a and e (Banerjee et al., 1985). The finite element model included a correction for the lateral confining stress generated by the rubber membrane used to enclose the sample (Rohlf, 1993). Input parameters for each triaxial test simulation are listed in table 3.

Results of the modeling for four triaxial tests are presented in figures 6 through 9 in terms of graphs containing (1) the stress path, (2) deviator stress versus axial and lateral strain, and (3) volumetric strain versus axial strain. Compressive strain is taken as positive.

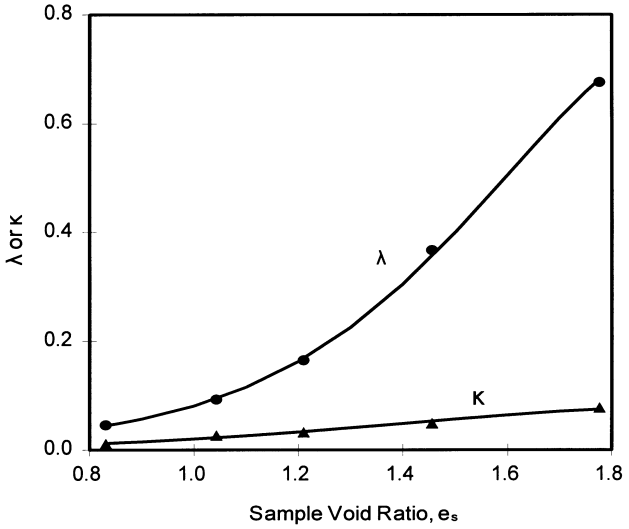

Figure 5. Lambda and kappa versus sample void ratio.

Table 3. Input parameters for matric–stress critical–state model

Parameter	Test			
	T116	T127	T139	T143
e_s	0.862	1.021	1.696	1.406
e_o	0.819	1.009	1.656	1.351
w	0.263	0.284	0.237	0.250
M	1.09	1.09	1.09	1.09
λ	0.050	0.088	0.607	0.310
κ	0.014	0.022	0.071	0.049
E (kPa)	7.2×10^3	2.9×10^3	1.7×10^3	1.7×10^3
ν	0.3	0.3	0.3	0.3
$[p_a + \overline{f(\mu)}]_o$ (kPa)	37.8	23.8	40.2	29.3
$\overline{f(\mu)}$ (kPa)	26.8	12.8	29.2	18.3

The stress path plots contain curves for the mean net stress, p_a, and mean net stress plus matric stress, $p_a + f(\mu)$. The predicted mean net stress in figures 6 through 9 was determined by subtracting f(μ) in table 1 from $[p_a + f(\mu)]$ calculated by the model. The decrease in slope of the stress paths near failure is due to the increase in lateral confining stress exerted by the latex membrane as the sample incurred lateral strain.

Figures 6a and 7a show that triaxial tests T116 and T127 approached the failure line, while figures 8a and 9a show that triaxial tests T139 and T143 were terminated prior to reaching failure. The difference in failure characteristics is apparently due to the large difference in void ratios. Samples T116 and T127 had sample void ratios of 0.862 and 1.021, respectively, while T139 and T143 had sample void ratios of 1.696 and 1.479, respectively (table 1). With higher initial void ratios, samples T139 and T143 required a much greater reduction in void ratio to reach critical state than samples T116 and T127. Thus, axial strains considerably greater than 25% would have been required to allow T139 and T143 to reach critical state. This observation is supported by figure 1, which shows that T139 and T143 were still experiencing a high rate of contraction at the termination of testing, while T116 and T127 were much closer to critical state where $d\varepsilon_v / d\varepsilon_s = 0$.

As indicated by figures 6 through 9, the model generally provided a satisfactory prediction of stress and axial, lateral, and volumetric strain for a wide range of soil conditions. For test T127, axial, lateral, and volumetric strain were somewhat under–predicted (fig. 7b); for T139 and T143, lateral strain was slightly under–predicted; and for T143 volumetric strain was over–predicted (figs. 8b and 9b).

The triaxial tests were successfully modeled using a constant matric stress. This result was not initially anticipated since the samples incurred large axial and volumetric strain, which might be expected to alter pore water meniscus radii, matric suction, and matric stress. However, constant matric stress for constant water content triaxial tests conducted at low confining pressure is consistent with the work of Adams and Wulfsohn (1997, 1998), where matric suction was found to be approximately constant for confining pressures less than 60 kPa. In contrast, constant water content triaxial tests at high confining pressure presented by Adams and Wulfsohn (1998) and Fredlund and Rahardjo (1993) show a large decrease in matric suction during shearing.

SUMMARY AND CONCLUSIONS

The modified Cam clay energy relationship was used to develop an analytic procedure for determining matric stress, the stress generated by matric suction. The procedure allows

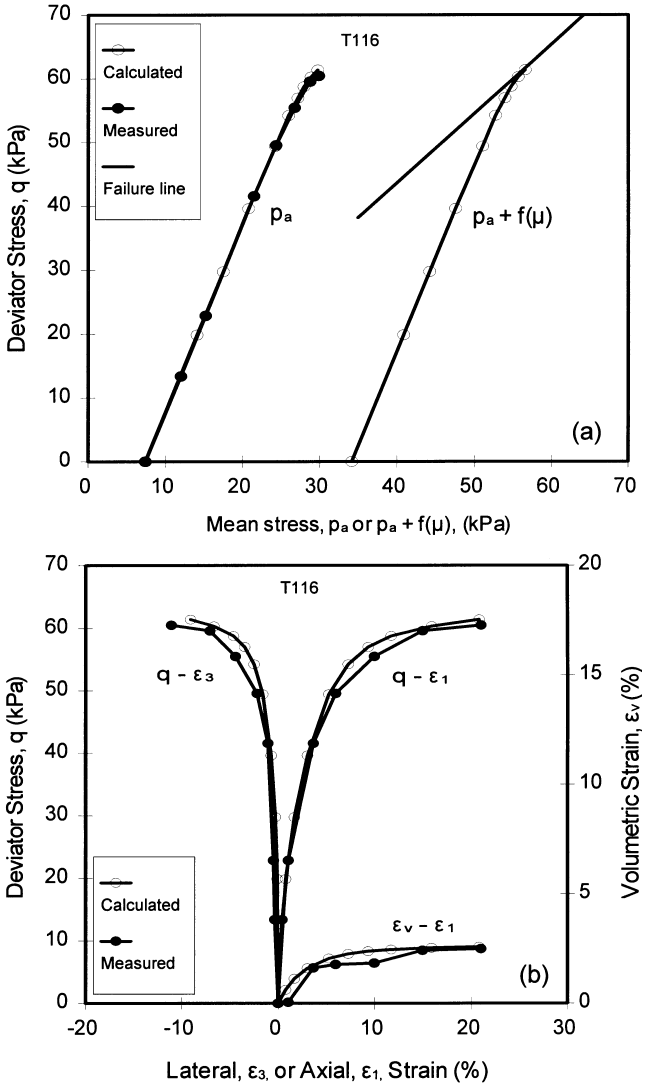

Figure 6. Comparison of measured and calculated triaxial test results for T116: (a) stress path, (b) deviator stress versus axial and lateral strain, and volumetric strain versus axial strain.

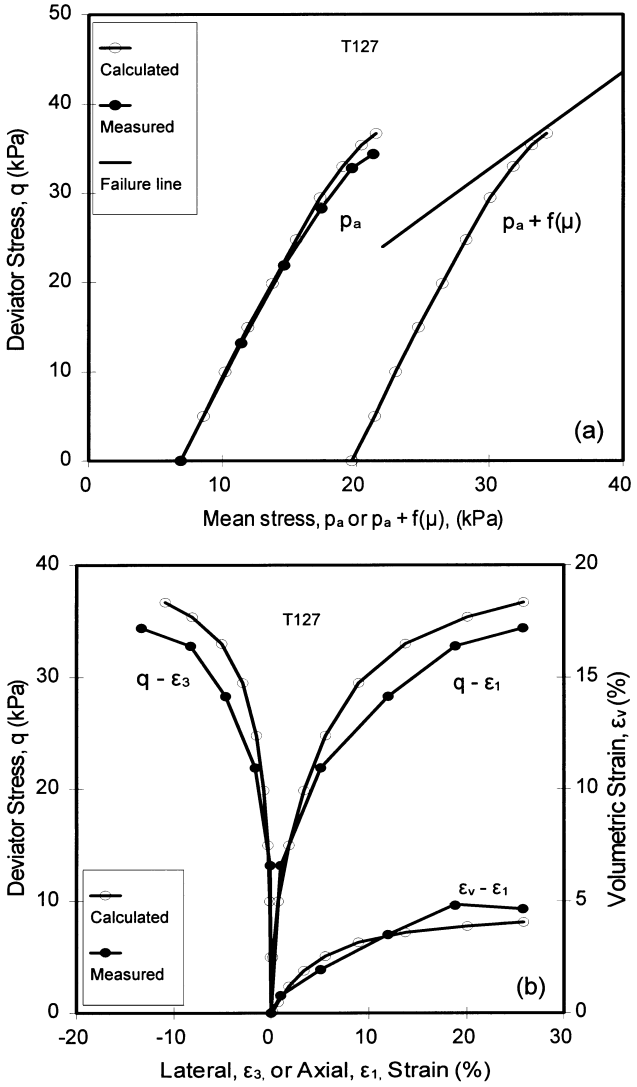

Figure 7. Comparison of measured and calculated triaxial test results for T127: (a) stress path, (b) deviator stress versus axial and lateral strain, and volumetric strain versus axial strain.

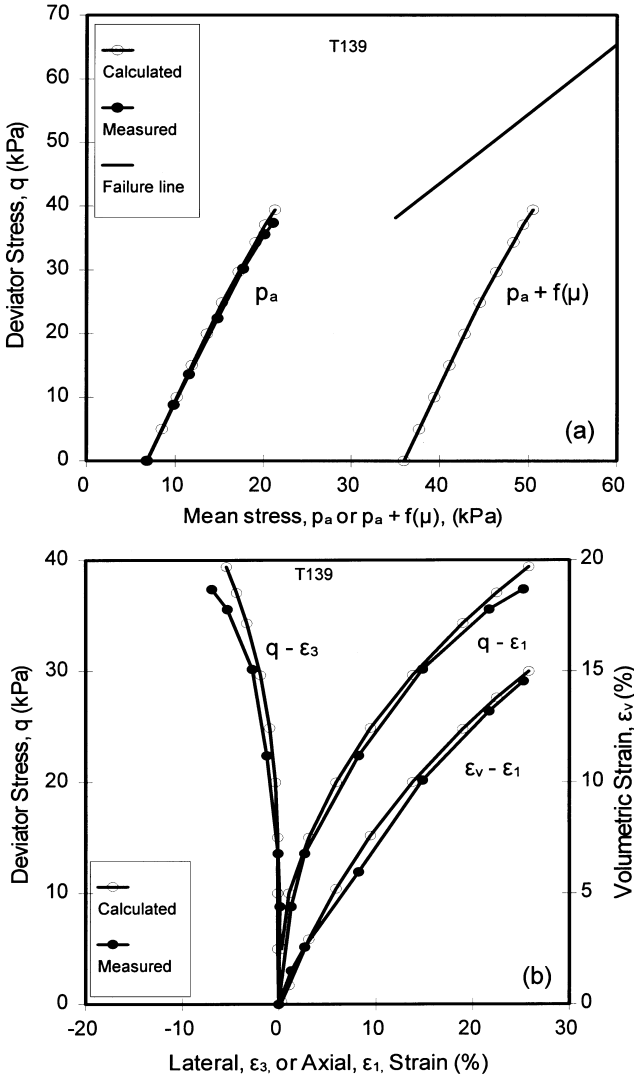

Figure 8. Comparison of measured and calculated triaxial test results for T139: (a) stress path, (b) deviator stress versus axial and lateral strain, and volumetric strain versus axial strain.

matric stress to be calculated at points along the stress path-where the deviator stress, mean net stress, dilation, and slope of the failure line are known.

For constant water content triaxial compression tests conducted at a low confining pressure of approximately 7 kPa, matric stress was found to be approximately constant at axial strains above 10% for samples with a large range in initial degree of saturation ($0.375 \leq S \leq 0.818$). Matric stress varied considerably for axial strains below 10%. This was likely due to elastic behavior at small and medium strains and inaccuracies in measuring small volumetric strains and in calculating dilation.

Matric stress was included in both shear and volume relationships in a critical–state soil model that employed the modified Cam clay yield function. Shear was modeled using a constant matric stress. Slopes of the normal compression and recompression lines were adjusted for matric stress using a state function that expressed matric stress as a function of void ratio and degree of saturation. The model provided a satisfactory prediction of deviator stress and axial, lateral, and volumetric strain. Results of the modeling indicate that the behavior of unsaturated soils at constant water content under triaxial compression with low confining stress can be successfully predicted using a critical–state model with a constant matric stress. Beyond predicting the behavior of unsaturated soil in triaxial tests, the model should be useful in analyzing channel bank deformation, channel erosion, wheel compaction and traction, and tillage tools.

Application of the energy procedure for determining matric stress to other forms of unsaturated triaxial testing, such as consolidated drained or consolidated undrained tests, should be possible. Application of the procedure to consolidated drained tests in which matric suction is held constant could provide useful information on the relationship between matric suction and matric stress.

REFERENCES

Adams, B. A., and D. Wulfsohn. 1997. Variation of the critical–state boundaries of an agricultural soil. *Euro. J. Soil Sci.* 48: 739–748.

_____. 1998. Critical–state behaviour of an agricultural soil. *J. Agric. Eng. Res.* 70: 345–354.

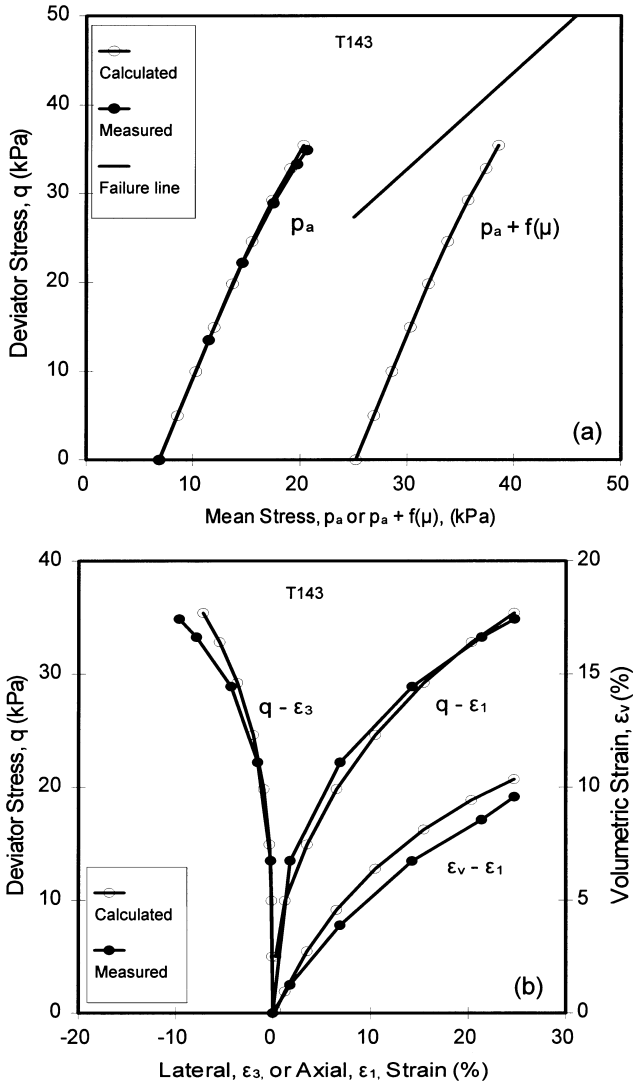

Figure 9. Comparison of measured and calculated triaxial test results for T143: (a) stress path, (b) deviator stress versus axial and lateral strain, and volumetric strain versus axial strain.

Alonso, E. E., A. Gens, and A. Josa. 1990. A constitutive model for partially saturated soils. *Geotechnique* 40(3): 405–430.

Banerjee, P. K., A. S. Stipho, and N. B. Yousif. 1985. A theoretical and experimental investigation of the behaviour of anisotropically consolidated clay. In *Developments in Soil Mechanics and Foundation Engineering*, vol. II: 1–41. London, U.K.: Applied Science.

Bishop, A. W. 1959. The principle of effective stress. *Teknisk Ukeblad* 106(39): 859–863.

Bishop, A. W., I. Alpan, G. E. Blight, and I. B. Donald. 1960. Factors controlling the strength of partly saturated cohesive soils. In *Research Conference on Shear Strength of Cohesive Soils Proceedings*, 503–532. Reston, Va.: American Society of Civil Engineers.

Bishop, A. W., and G. E. Blight. 1963. Some aspects of effective stress in saturated and partly saturated soils. *Geotechnique* 13(3): 177–197.

Blight, G. E. 1967. Effective stress evaluation for unsaturated soils. *Proc. Am. Soc. Civ. Engrs* 93(SM2): 125–148.

Burland, J. B. 1965. Some aspects of the mechanical behaviour of partly saturated soils. In *Proceedings of a Symposium on Moisture Equilibria and Moisture Changes in Soils Beneath Covered Areas*, 270–278. Sydney, Australia: Butterworths.

Das, B. M. 1983. *Advanced Soil Mechanics*. New York: McGraw–Hill.

Fredlund, D. G., and N. R. Morgenstern. 1977. Stress state variables for unsaturated soils. *J. Geotech. Eng., ASCE* 103 (GT5): 447–466.

Fredlund, D. G., N. R. Morgenstern, and R. A. Widger. 1978. The shear strength of unsaturated soils. *Canadian Geotech. J.* 15(3): 313–321.

Fredlund, D. G., and H. Rahardjo. 1993. *Soil Mechanics for Unsaturated Soils*. New York: John Wiley.

Jennings, J. E., and J. B. Burland. 1962. Limitations to the use of effective stress in partly saturated soils. *Geotechnique* 12(2): 125–144.

Karube, D. 1988. New concept of effective stress in unsaturated soil and its proving test. In *Advanced Triaxial Testing of Soil and Rock*, 539–552. R. T. Donaghe, R. C. Chaney, and M. L. Silver, eds. ASTM STP 977. West Conshohocken, Pa.: American Society for Testing and Materials.

Lloret, A., and E. E. Alonso. 1980. Consolidation of unsaturated soils including swelling and collapse behavior. *Geotechnique* 30(4): 449–477.

Matyas, E. L., and H. S. Radhakrishna. 1968. Volume change characteristics of partially saturated soils. *Geotechnique* 18(4): 432–448.

Rohlf, R. A. 1993. Groundwater flow and elastoplastic stress–strain modeling of channel bank failure. Ph.D. dissertation. Lexington, Ky: Univ. of Kentucky, Dept. of Civil Engineering.

Rohlf, R. A., B. J. Barfield, and G. K. Felton. 1994. Groundwater flow and elastoplastic stress–strain model for cohesive soils with application to channel bank stability. Research Report No. 191, Lexington, Ky: Univ. of Kentucky Water Resources Institute.

_____. 1997. Ultimate strength matric stress relationship. *J. Geotech. and Geoenv. Eng., ASCE* 123(10): 938–947.

Rohlf, R. A., X. Zeng, and L. G. Wells. 2000. Simulating deformation of an excess spoil fill. In *Advances in Unsaturated Geotechnics*, 303–317.C. D. Shackelford, S. L. Houston, and N. Chang, eds. Geotechnical Special Publication No. 99. Reston, Va.: American Society of Civil Engineers.

Romkens, M. J. M., R. E. Phillips, J. M. Selim, and F. D. Whisler. 1985. Physical characteristics of soils in the southern region – Vicksburg, Memphis, Maury Series. Bulletin No. 266. Southern Cooperative Series. Mississippi State, Miss.: Mississippi Agricultural and Forestry Experiment Station.

Roscoe, K. H., and J. B. Burland. 1968. On the generalized stress–strain behaviour of "wet" clay. In *Engineering Plasticity*, 535–609. J. Heyman and F. A. Leckie, eds. Cambridge, U.K.: Cambridge University Press.

Schofield, A. N., and C. P. Wroth. 1968. *Critical State Soil Mechanics.* London, U.K.: McGraw–Hill.

Toll, D. G. 1990. A framework for unsaturated soil behaviour. *Geotechnique* 40(1): 31–44.

Wheeler, S. J., and V. Sivakumar. 1995. An elasto–plastic critical state framework for unsaturated soil. *Geotechnique* 45(1): 35–53.

Whitlow, R. 1990. *Basic Soil Mechanics.* 2nd ed. Essex, U.K.: Longman Scientific and Technical.

Wood, D. M. 1990. *Soil Behaviour and Critical State Soil Mechanics.* Cambridge, U.K.: Cambridge University Press.

NOMENCLATURE

The following symbols are used in this article:

A_w = area of saturated pore space, L^2
a_i = regression coefficient
b_i = regression coefficient
C_c = compression index
c_i = regression coefficient

D = dilatancy
$\overline{D}$ = average dilatancy
d_i = regression coefficient
E = Young's modulus, F/L^2
e = void ratio
e_o = initial void ratio
e_s = void ratio at sample formation
f(μ) = matric stress, F/L^2
$f(\mu)_o$ = initial matric stress, F/L^2
$\overline{f(\mu)}$ = average matric stress, F/L^2
LL = liquid limit
M = slope of failure line in q–p stress space
M_a = slope of the failure line in q–p stress space with respect to mean net stress
m_v = coefficient of volume compressibility, 1/(F/L^2)
PI = plastic index
$\underline{p_a}$, p = mean net stress, F/L^2
$\overline{p_a}$ = average mean net stress, F/L^2
p_{ao} = initial mean net stress, F/L^2
p_1, p_2 = mean net stress at failure, F/L^2
q = deviator stress, F/L^2
q_f, q^f = deviator stress at failure, F/L^2
q_1, q_2 = deviator stress at failure, F/L^2
S = degree of saturation
S_s = degree of saturation at sample formation
S_{ij} = deviatoric stress tensor, F/L^2
T = surface tension, F/L^2
u_a = pore air pressure, F/L^2
$u_a - u_w$ = matric suction, F/L^2
u_w = pore water pressure, F/L^2
w = gravimetric water content
x = length along air–water meniscus, L
δ_{ij} = Kronecker delta
ε_s = shear strain
ε_v = volumetric strain
ε_s^p = plastic shear strain
ε_v^p = plastic volumetric strain
ε_1 = triaxial axial strain
ε_3 = triaxial lateral strain
η = stress ratio
$\overline{\eta}$ = average stress ratio
κ = slope of swelling and recompression line
κ_a = slope of swelling and recompression line with respect to mean net stress
λ = slope of normal consolidation line
λ_a = slope of the normal consolidation line with respect to mean net stress
μ = matric suction, F/L^2
ν = Poisson's ratio
σ = normal stress, F/L^2
$\overline{\sigma_{ij}}$ = intergranular stress tensor, F/L^2
$\sigma - u_a$ = net normal stress, F/L^2
σ_{ij} = total stress tensor, F/L^2
σ_1 = major principal stress, F/L^2
σ_3 = minor principal stress, F/L^2